Supplemental material

Pineda et al., https://doi.org/10.1083/jcb.201907178

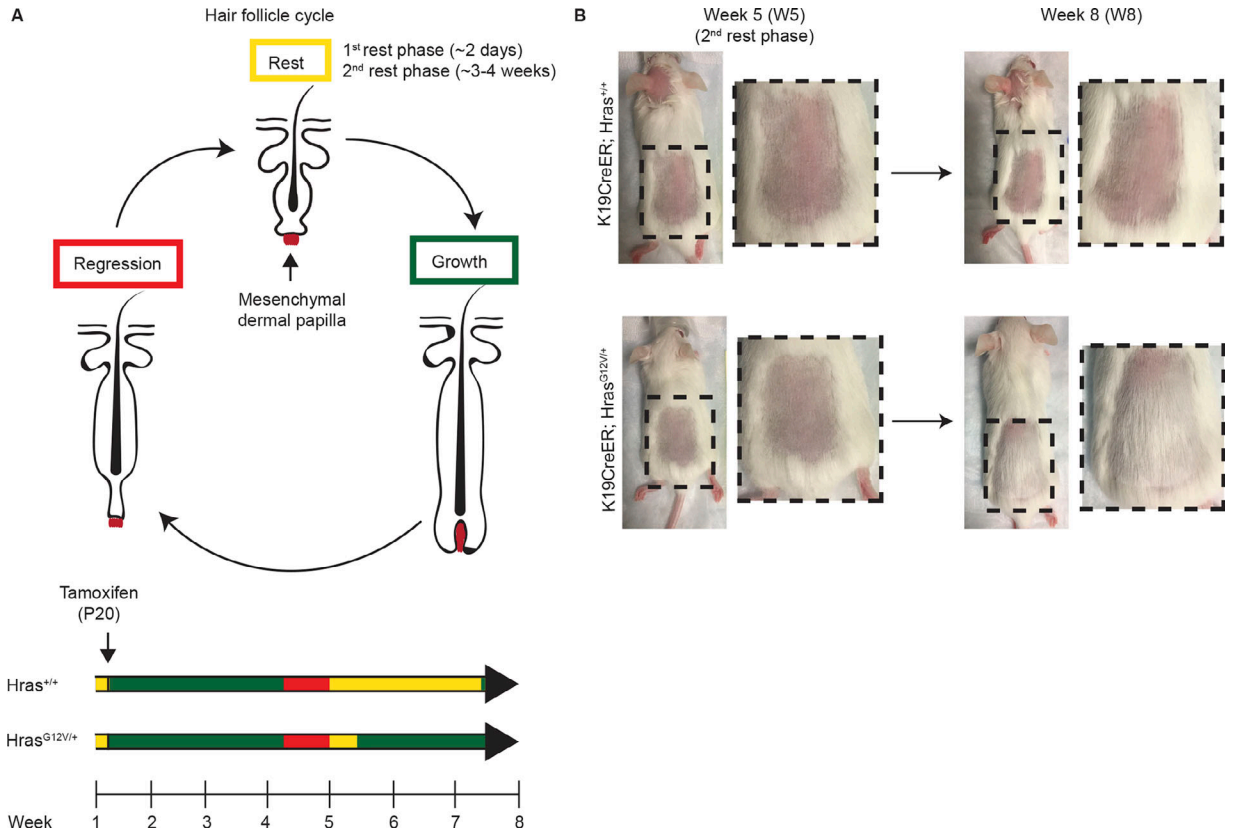

Figure S1. **Hras activation promotes faster hair growth. (A)** Top: Hair follicle cycling cartoon. Bottom: Cartoon depicting the faster growth reentry of K19CreER;Hras$^{G12V/+}$ follicles compared with wild-type follicles. Yellow, rest; green, growth; red, regression. **(B)** Photographs of representative K19CreER; Hras$^{+/+}$ (top) and K19CreER;Hras$^{G12V/+}$ (bottom) mice who had their backs shaved at week 5 after tamoxifen during the second rest phase. Photographs taken of the same mice at week 8 reveal faster hair growth in the Hras mutant mice. Assay performed on *n* = 3 K19CreER;Hras$^{+/+}$ and *n* = 3 K19CreER;Hras$^{G12V/+}$ mice.

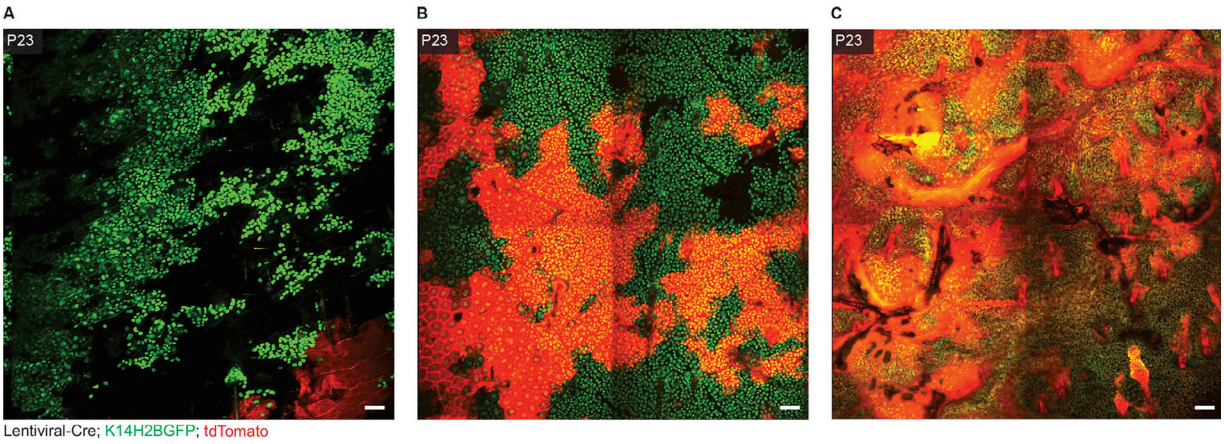

Figure S2. **Lentiviral Cre titer can be adjusted to achieve variable degrees of mosaicism.** Injection of lentiviral Cre into K14H2BGFP; tdTomato mice at low (A), medium (B), and high (C) titers can create varying levels of activation as assayed by tdTomato recombination. All scale bars represent 50 µm.

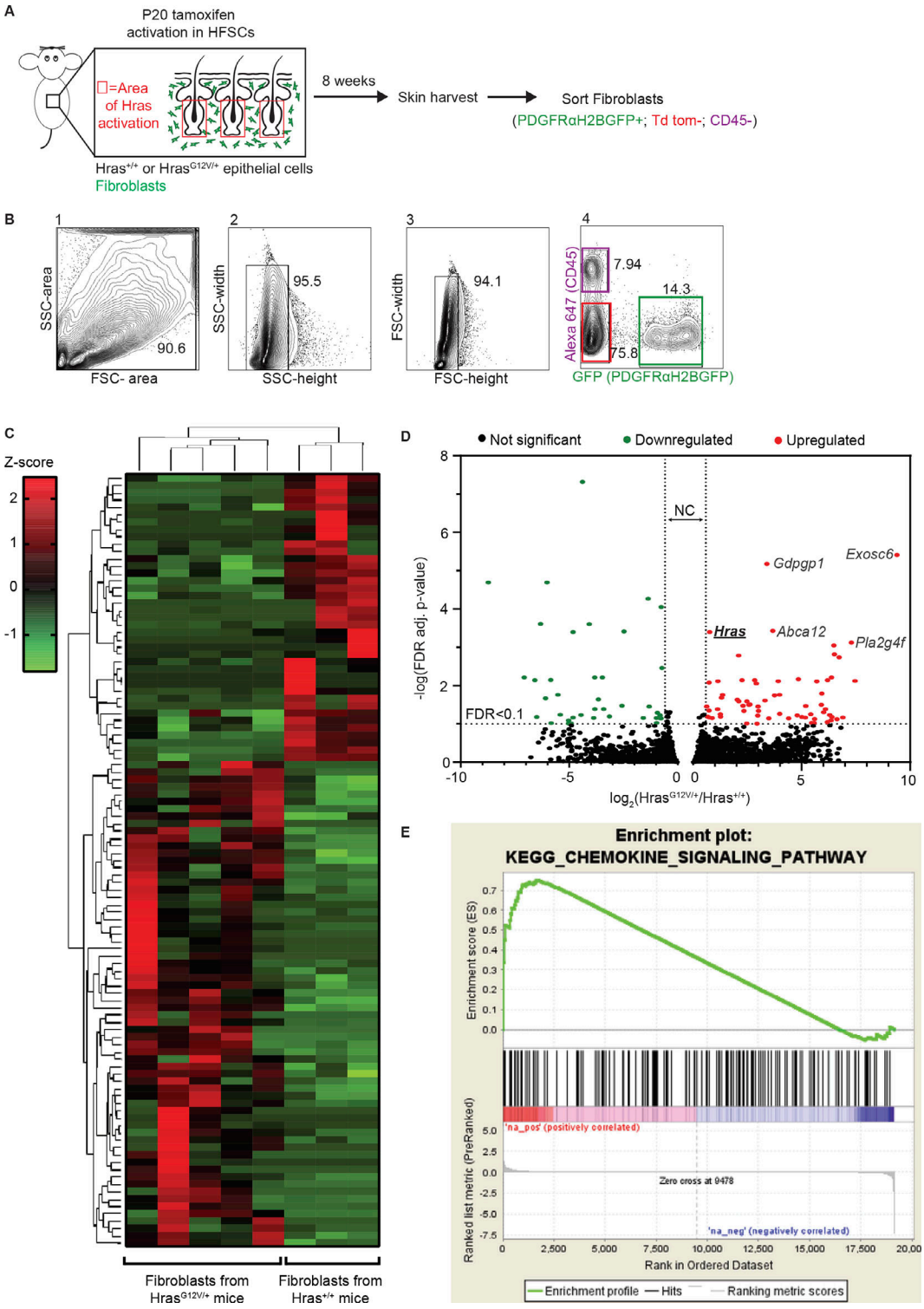

Figure S3. **Epithelial Hras activation nonautonomously alters gene expression in the surrounding mesenchyme. (A)** Cartoon depiction of mouse sorting strategy and time frame for RNA-seq analysis. **(B)** Example of the FACS strategy from one representative mouse depicting the initial gating of all living cells using forward scatter (FSC) and side scatter (SSC) area, width, and height (1–3), the gating of individual populations based on Alexa Fluor 647 positivity (CD45$^+$ cells, immune), tdTomato positivity (Pe-Texas Red+ cells, epithelial), and GFP positivity (PDGFRα+ cells, fibroblasts, 4). **(C)** Heatmap and hierarchical clustering of RNA-seq data demonstrates differences in expression between fibroblasts sorted from three Hras$^{+/+}$ mice versus five Hras$^{G12V/+}$ mice, with mice of the same genotype clustering together (filtered gene list based on FDR <0.1). **(D)** Volcano plot depicting genes both significantly (FDR < 0.1) up-regulated (red, 66) and down-regulated (green, 39) in fibroblasts from Hras$^{G12V/+}$ mice compared with controls. NC indicates no fold change (|fold change| < 1.5). The top five most statistically significant positively up-regulated genes in the fibroblasts from Hras mutant mice are labeled, including Hras (bold and underlined). **(E)** Gene set enrichment analysis positive enrichment plot for the chemokine signaling pathway in fibroblasts from Hras$^{G12V/+}$ mice compared with controls (FDR q-value = 0.1960, normalized enrichment score = 1.3609).

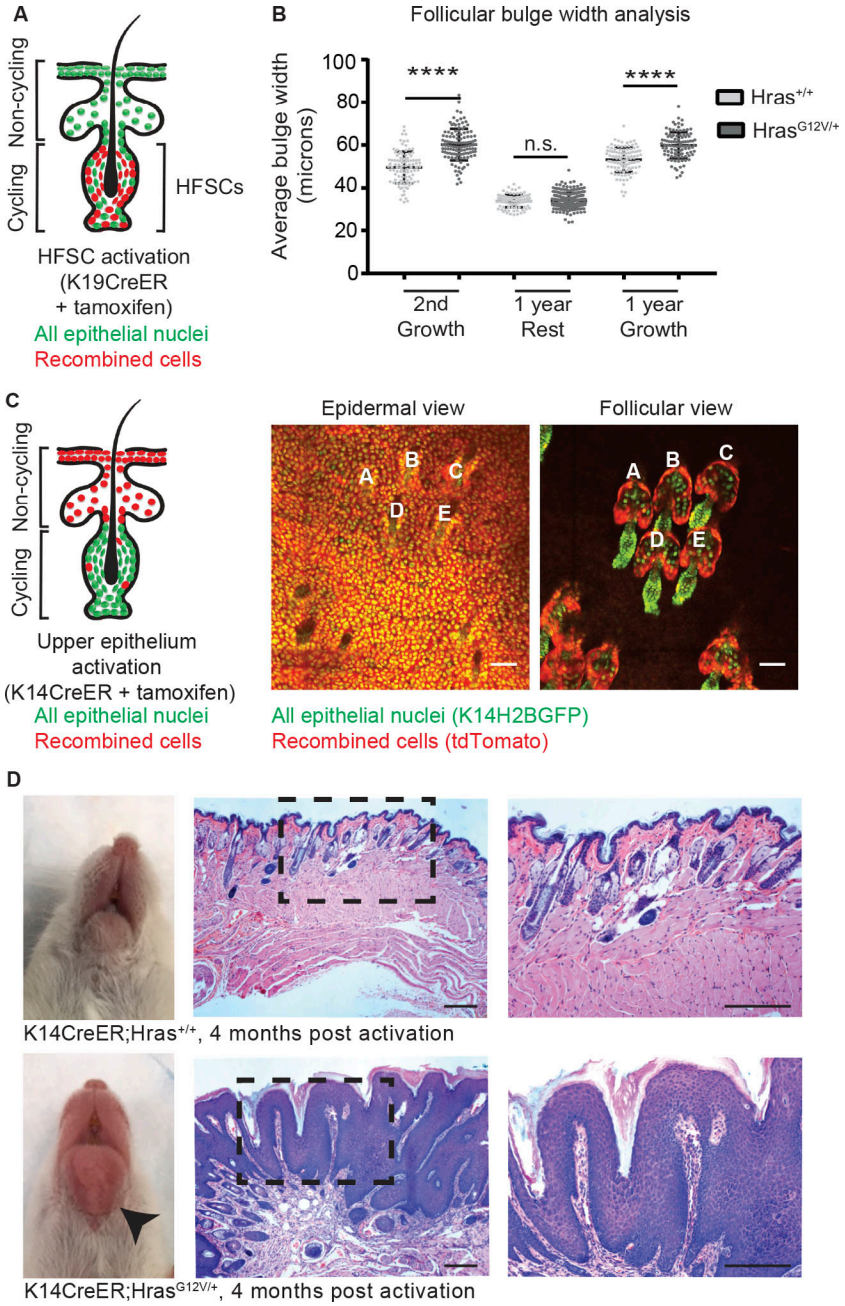

Figure S4. **The hair follicle has an enhanced ability to tolerate mutant cells compared with the epidermis.** All epithelial nuclei are in green (K14H2BGFP), and recombined cells are in red (tdTomato). **(A)** Cartoon schematic depicting targeted Cre activation to HFSCs using a K19CreER system. **(B)** Follicular bulge width analysis of hair follicles during the second growth phase, 1-yr growth phase, and 1-yr rest phase in $Hras^{+/+}$ and $Hras^{G12V/+}$ mice reveals continuous correction of follicular hyperthickening. For all significance values, ****, $P < 0.0001$ as determined by an unpaired, two-tailed *t* test. Error bars indicate standard deviation. **(C)** Left: Cartoon schematic depicting targeted Cre activation to the upper, noncycling epithelium using a K14CreER system. Right: Two-photon images of the epidermis and hair follicles of a K14CreER;K14H2BGFP;tdTomato mouse injected with 2 mg tamoxifen at P20 reveals targeted activation to the noncycling epithelium. Scale bars represent 50 µm. **(D)** Photographs and hematoxylin and eosin images of K14CreER;$Hras^{+/+}$ (top) and K14CreER;$Hras^{G12V/+}$ (bottom) mice reveal the Hras mutant mice develop benign papillomas (*n* = 4/4 K14CreER;$Hras^{G12V/+}$ mice developed benign papillomas, while *n* = 0/4 K14CreER;$Hras^{+/+}$ did in the same time frame). Scale bars represent 200 µm.

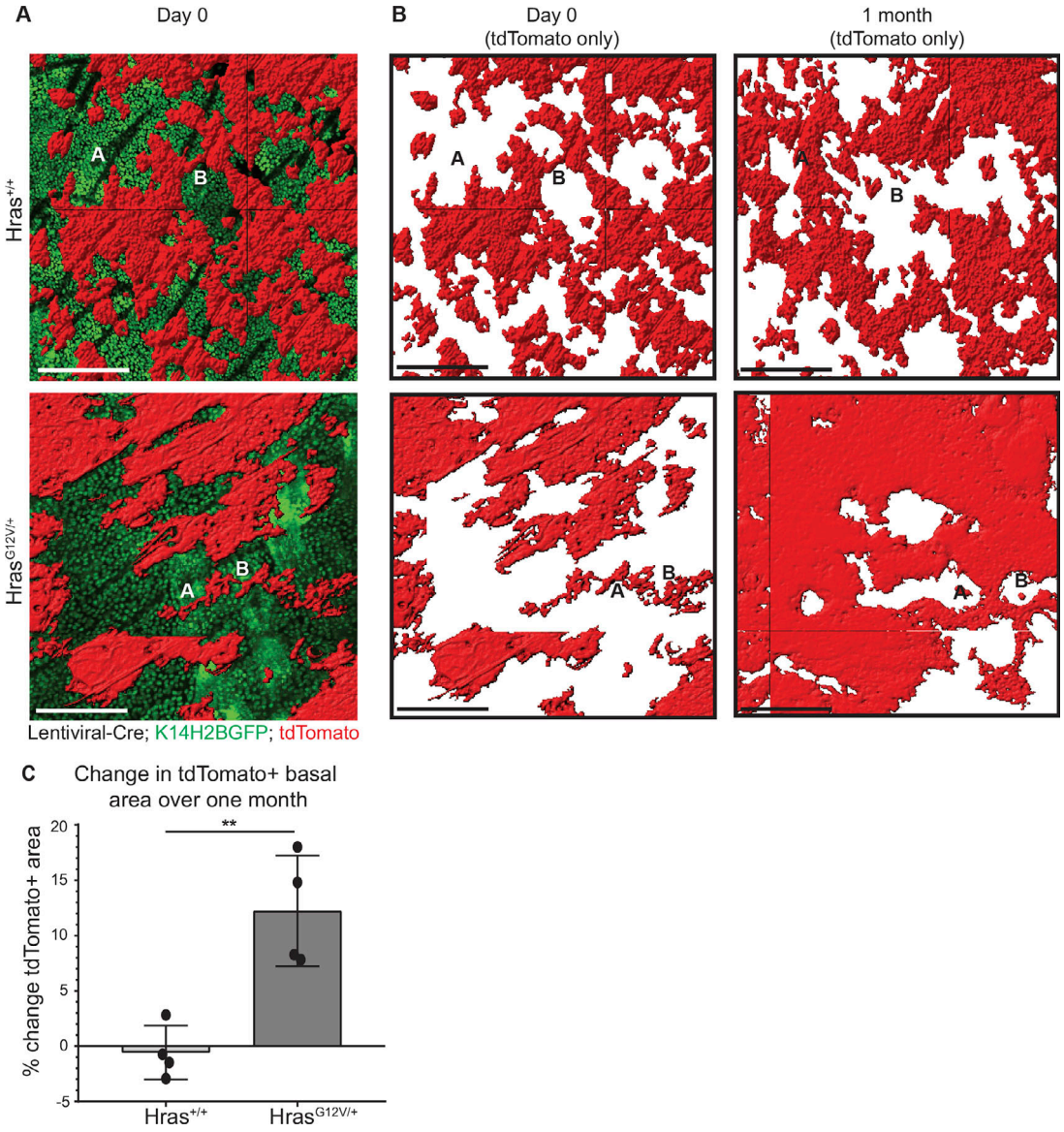

Figure S5. **Hras mutant cells outcompete wild-type neighbors in the epidermis.** All epithelial nuclei are in green (K14H2BGFP), and recombined cells are in red (tdTomato). **(A)** Two-photon images of an LV-Cre;$Hras^{+/+}$ epidermis (top) and an LV-Cre;$Hras^{G12V/+}$ epidermis (bottom) at day 0 (P23). The tdTomato cells are projected as a volumetric mask, and hair follicle entry points are labeled A and B as reference points in each image. **(B)** Two-photon images of the same epidermal images seen in A with only the tdTomato mask projected in red at day 0 and 1 mo later. The images reveal substantial expansion of the tdTomato in the Hras mutant (bottom) compared with the wild type (top) over time. All scale bars represent 50 µm. **(C)** Quantification of tdTomato$^+$ basal area expansion over 1 mo reveals a significant expansion in the $Hras^{G12V/+}$ epidermis compared with the $Hras^{+/+}$ control (n = 4 $Hras^{+/+}$ and 4 $Hras^{G12V/+}$ mice, P = 0.0037). Error bars indicate standard deviation. For significance value, **, P < 0.01.

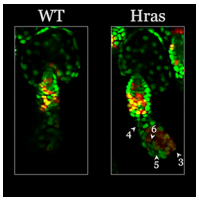

Video 1. **The Hras mutant follicle has more mitotic events than wild-type controls (related to Fig. 1).** All epithelial nuclei are labeled in green (K14H2BGFP), and all recombined cells are labeled in red (tdTomato). Representative z-stacks (every 2 µm) through ears of live K19CreER;$Hras^{+/+}$ (left) and K19CreER;$Hras^{G12V/+}$ (right) mice reveal an increased number of mitotic events in Hras mutant hair follicles. Numbered arrowheads each point to a distinct mitotic event.

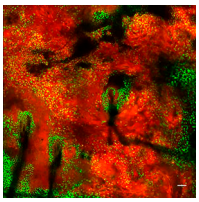

Video 2. **cSCC of a double-mutant mouse (related to Fig. 3).** All epithelial nuclei are labeled in green (K14H2BGFP), and all recombined cells are labeled in red (tdTomato). A representative z-stack (every 2 µm) through the cSCC tumor of a K19CreER; $Hras^{G12V/+}$;$Alk5^{-/-}$ mouse reveals that the $tdTomato^{+}$ cells, originally activated in the cycling portion of the hair follicle, have infiltrated the epidermis. Scale bar represents 50 µm.